Uncertainty quantification of low-speed fan noise

By J. Christophe†‡, M. Sanjose‡, S. Moreau‡, J.A.S. Witteveen AND G. Iaccarino

Uncertainty quantification (UQ) has been achieved for the first time on the self-noise prediction of a low-subsonic axial fan. Realistic 5% and 4% errors are introduced on the volume flow-rate and the rotational speed, respectively, and a set of 81 Reynolds-Averaged Navier-Stokes (RANS) simulations of the fan mounted on an axisymmetric test plenum has been simulated at Clenshaw-Curtis points. By using the Stochastic Collocation method, extractions from this set of RANS simulations, and reconstructions of the wall-pressure fluctuations with two different models, uncertainties on global performances, wall-pressure distribution, and far-field noise spectra were obtained. The stochastic mean spectra are dominated by the tip strip and compare well with experimental data. Larger uncertainties are seen in the hub and tip regions, where large flow detachment and recirculation appear. Flow rate variations yield larger uncertainties on sound than do rotational speed variations.

1. Introduction

In modern rotating machines, significant effort has been expended to reduce or eliminate annoying discrete tones, either by passive devices or by active noise control. The next challenge is then to reduce the broadband contribution to decrease the overall noise level and meet new environmental noise regulations. The self-noise generated by rotating machines, caused by the scattering of boundary-layer pressure fluctuations into acoustic waves at the trailing-edge of any lifting surface, is a problem in many applications such as in wind turbines, laptop, or automotive cooling fan systems or in heating, ventilating and air conditioning devices. However, an accurate prediction of the sound by a low-speed fan system still remains a daunting task by a direct computation (compressible LES for instance), even in the near field of the blade.

In the present study, the noise predictions then rely on a strip theory combined with an acoustic analogy (Lighthill 1952), originally developed by Schlinker & Amiet (1981) for helicopters rotors trailing-edge noise, and extended to finite chord lengths and general three-dimensional gusts by Roger & Moreau (2005), and applied to low-speed fans by Moreau & Roger (2007). The main input required by the theory is the wall-pressure trailing-edge spectrum that is usually obtained by means of unsteady aerodynamic flow computations or experiments. In order to further reduce the computational costs, approaches that model the pressure fluctuations needed for an acoustic analogy from steady RANS are often used (Casalino *et al.* 2010; Glegg *et al.* 2010; Rozenberg *et al.* 2010; Remmler *et al.* 2010). These methods add more levels of modeling and the associated epistemic uncertainties grow, which may make the final acoustic prediction inaccurate and unreliable. The complete methodology, from RANS computation to noise prediction,

† Environmental and Applied Fluid Dynamics Dept., von Karman Institute for Fluid Dynamics, Brussels, Belgium
‡ Université de Sherbrooke, Sherbrooke QC, J1K2R1, Canada

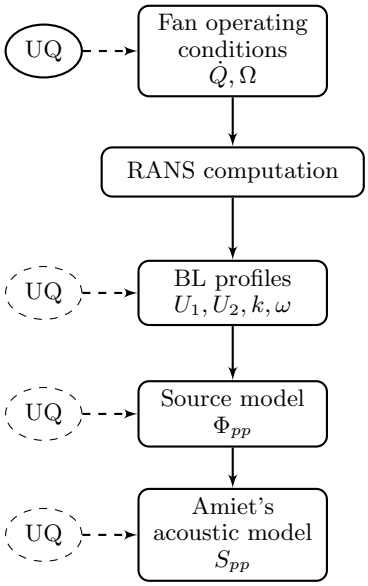

FIGURE 1. Uncertainty quantification methodology.

FIGURE 2. H380EC1 low-speed fan.

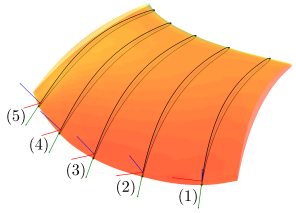

FIGURE 3. Extraction profiles on the blade surface and corresponding reference frames for the extraction points near the trailing-edge.

is described in Section. 2. It can be seen as an extension of the trailing-edge noise models based on steady RANS simulations applied to a controlled-diffusion (CD) airfoil (Moreau 2009; Christophe *et al.* 2010), to a full automotive axial fan. Two main parameters are controlling its operating condition: the volume flow-rate through the fan and the rotational speed. Uncertainty quantification (UQ) on both parameters are first considered in Section. 3. In Section. 4, the influence of all the parameters introduced in the RANS information extractions, the wall-pressure reconstruction, and the noise propagation is analyzed in a multi-parameters UQ study.

2. Methodology

The approach to UQ to compute fan trailing-edge noise is illustrated in Figure. 1. As in (Christophe *et al.* 2012), a RANS computation of flow in a blade passage of the fan is first performed. The input parameters for this computation are the volume flow rate $\dot{Q}$ and the rotational speed Ω. Both parameters are considered as main parameters for the uncertainty quantification on fan operating conditions (solid circle in Figure. 1). The computational setup, defined by the fan and tip gap are directly taken from the design of the experimental setup and is therefore considered as a minor source of possible error on the final sound prediction results. From this RANS computation, the primitive variables are extracted through a boundary-layer profile at the trailing-edge of the fan blade, at five radial positions along the blade span, illustrated in Figure. 3. Those variables are then used to reconstruct wall-pressure fluctuation spectra Φ_{pp}. Finally, the latter power spectral densities provide the far-field sound spectrum S_{pp} in the extended Amiet's theory (Roger & Moreau 2005). A second source of uncertainty can be introduced in the present methodology (dashed circles in Figure. 1) corresponding to all the parameters involved in the data extraction of the boundary-layer profiles, in the wall-pressure recon-

struction models and in the acoustic propagation model. Those parameters are defining a multi-parameter problem that are studied in Section. 4.

2.1. *Geometry and numerical setup*

The symmetric rotor considered here is a typical automotive cooling fan, illustrated in Figure. 2, with 9 blades designed for a best efficiency point at a volume flow-rate of 2500 m^3/h at a rotational speed of 2500 rpm. The rotor is flush mounted on a plenum walls from which the static pressure rise across the fan is measured. The available experimental data include overall performances and acoustic power measurements at several flow-rates and rotational speeds obtained in a reverberant wind tunnel. The plenum is assumed axisymmetric so that a single blade passage, including the actual tip gap, is modeled and matching nodes are used at the periodic boundary conditions (Moreau *et al.* 2012). The flow is modelled with RANS computations using the shear-stress-sransport (SST) $k-\omega$ turbulence model in the ANSYS CFX 14 solver. The mesh has a total of 5.1 million hexahedral elements and is refined in the boundary-layers around the blade to reach dimensionless distances to the wall y^+ less than 5 in the trailing-edge region, where presently most of the sound production occurs. The volume flow-rate is set on the inlet surface of the plenum. The average pressure on the outlet surface is set to the reference pressure. Low-dissipation second-order numerical schemes are used for the flow variables (velocity and pressure) and a first-order scheme for the transport of turbulent quantities. To yield to repeatable and consistent results, once the maximum convergence is reached, solutions are averaged over the last 500 iterations.

2.2. *Models for wall-pressure reconstruction and acoustic predictions*

From the RANS mean flow, the wall-pressure fluctuation spectra Φ_{pp} are reconstructed. First, Rozenberg's (YR) model (Rozenberg *et al.* 2010) uses only integrated boundary-layer parameters and reads

$$\frac{\Phi_{pp}(\omega_a)\,U_e}{\tau_w^2\,\delta} = \frac{(C_2\,\Pi\,\beta_C + C_4)\left(\dfrac{\omega_a\delta}{U_e}\right)^2}{\left[\left(\dfrac{\omega_a\delta}{U_e}\right)^{0.75} + C_1\right]^{3.7} + \left[C_3 R_T^{-0.57}\left(\dfrac{\omega_a\delta}{U_e}\right)\right]^7}, \tag{2.1}$$

where Clauser's parameter is $\beta_C = (\Theta/\tau_w)(dp/dx)$; Coles' parameter Π is given by the implicit law of the wake: $2\,\Pi - \ln(1+\Pi) = \frac{\kappa\,U_e}{u_\tau} - \ln\left(\frac{\delta^\star\,U_e}{\nu}\right) - \kappa\,C - \ln\kappa$; and R_T is $\frac{u_\tau\delta}{\nu}\sqrt{C_f/2}$. The numerical parameters $C_1 = 0.5$, $C_2 = 1.404$, $C_3 = 1.1$, and $C_4 = 4.68$ are considered later as uncertain parameters.

Secondly, using Panton & Linebarger's (PL) model (Panton & Linebarger 1974), Remmler *et al.* (2010) derived an expression for the wall-pressure spectrum

$$\Phi_{pp}(\omega_a) = 8\rho^2 \iiint_0^\infty \frac{k_a^1(\omega_a)^2}{k_a(\omega_a)^2}\exp^{-k_a(\omega_a)(y+\hat{y})}\,S_{22}(y,\hat{y},\omega_a)\frac{\partial U_1}{\partial y}\frac{\partial U_1}{\partial \hat{y}}dyd\hat{y}dk_a^3, \tag{2.2}$$

with the energy spectrum of the vertical velocity fluctuations:

$$S_{22}(y,\hat{y},\omega_a) = \frac{\bar{u_2'}(y)\bar{u_2'}(\hat{y})}{\pi^2}\Lambda^2 \iint_0^\infty R_{22}\cos(\alpha\,k_a^1(\omega_a)r_1)\cos(\alpha k_a^3 r_3)dr_1dr_3. \tag{2.3}$$

The model therefore uses the streamwise mean velocity profile $U_1(y)$ and the crosswise velocity fluctuation profile $u_2'(y)$. Both velocities and the velocity correlation length scale

Λ are calculated from the RANS outputs. The velocity correlation function R_{22} and the scale anisotropy factor α need to be modelled. The integration is performed with a Monte Carlo method using importance sampling for enhancing convergence (Remmler *et al.* 2010).

As shown by Roger & Moreau (2005), the trailing-edge noise can then be obtained by iteratively solving scattering problems at the airfoil edges. The random predicted sound field in the midspan plane at a given observer location $\vec{x} = (x_1, x_2, 0) = (R, \theta, z = 0)$ and for a given radian frequency ω_a (or wavenumber k_a) then reads

$$S_{pp}(\vec{x}, \omega_a, \theta) = \left(\frac{\sin\theta}{2\pi R}\right)^2 (k_a C)^2 \frac{L}{2} |\mathcal{L}|^2 \Phi_{pp}(\omega_a, \theta) l_y(\omega_a), \tag{2.4}$$

where l_y is the spanwise correlation length defined by $l_y = \frac{b_c U_c}{\omega_a}$ with $b_c = 1.47$. The radiation integral $\mathcal{L}$ involving both the free stream velocity U_e and the convection speed as parameters can be found in Roger & Moreau (2005).

In case of rotation, the far-field noise PSD of a low solidity fan with B independent blades is given by an integration over all possible azimuthal positions of the single airfoil formulation (2.4) (Schlinker & Amiet 1981):

$$S_{pp}(\mathbf{X}, \omega_a) = \frac{B}{2\pi} \int_0^{2\pi} \frac{\omega_e(\Psi)}{\omega_a} S_{pp}^{\Psi}(\mathbf{x}, \omega_e) d\Psi. \tag{2.5}$$

The factor $\omega_e(\Psi)/\omega_a$ accounts for Doppler effects caused by the rotation. In order to take into account the variation of the flow along the airfoil span, the blade is split in 5 segments, as in Christophe *et al.* (2012), and the total radiated sound is then the summation of the sound emitted by each airfoil strip.

2.3. *UQ method and determination of random variables*

Among the classical methods for stochastic differential equations, the stochastic collocation (SC) method has shown its reliability and efficiency compared to classical Monte Carlo (MC) methods in a previous study on uncertainty quantification on the CD airfoil (Christophe *et al.* 2010). The latter prescribes ensemble random inputs to the equations to solve and then collect their ensemble solution realizations. The SC method approximates the stochastic output of a model by projecting it onto a Lagrange polynomial basis, and the stochastic solution is evaluated at a discrete set of points, according to a nested Clenshaw-Curtis quadrature sharing abscissa for different accuracy of interpolation.

As introduced above, only the parameters defining the operating conditions are considered for uncertainty quantification in a first step. The volume flow rate is defined with a 5% error bound around 2500 m^3/h. The variation of this variable mainly depends on discrete events, such as dirt in the upstream heat exchanger, quality and nature of the fan, and cooling module assembly and manufaturing. A uniform probability density function (PDF) is therefore considered. The variation of rotational speed mainly depends on the motor manufacturing quality and is thus defined by a Gaussian PDF. A usual process dispersion for automotive electrical motors is $\pm$100 rpm. The rotational speed is thus defined with a 4% error bound around 2500 rpm. For these two variables considered independently, a set of 9 RANS computations are determined using a Clenshaw-Curtis quadrature. For the two-dimensional uncertainty quantification involving both variables, a full tensor grid of 81 RANS computations is used. In a second step, using the deterministic RANS computations, 9 parameters involved in the YR model are considered for

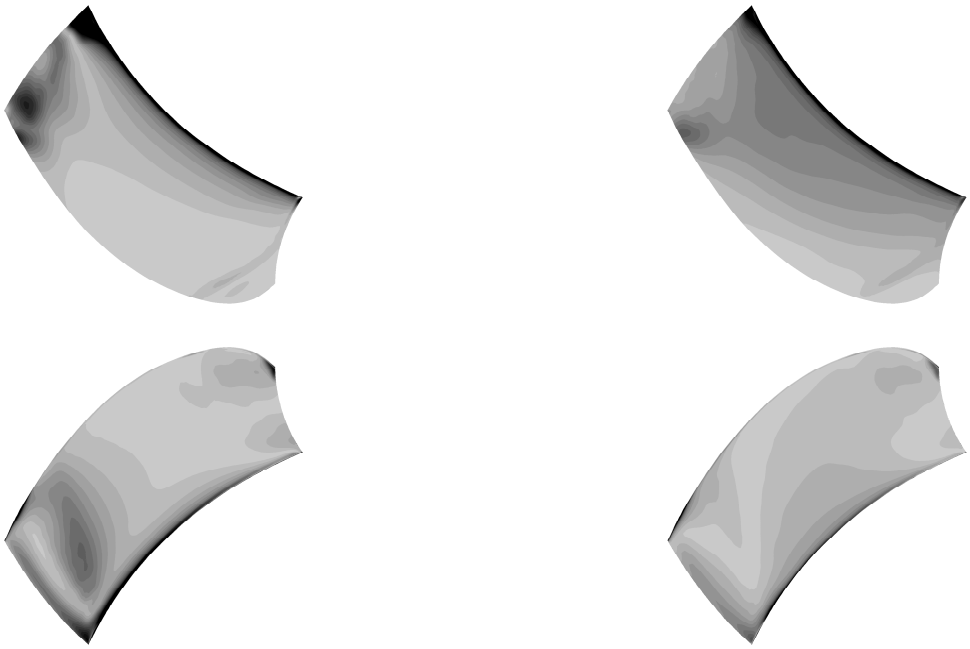

FIGURE 4. Iso-contours of the standard deviation of the static pressure on (top) suction side (contour levels [0:2:40]) and (bottom) pressure side (contour levels [0:1:20]). (Left) Variation of the volume flow rate and (right) variation of the rotational speed.

uncertainty quantification: the distance from the trailing-edge along the chord-line to extract the boundary-layer profile (2% chord), the C_1 to C_4 coefficients of the YR model, the density ($\rho = 1.185$ kg/m^3), the speed of sound ($c_0 = 340$ m/s), Corcos' constant b_c, and the convection velocity coefficient ($U_e/U_c = 1.43$). All parameters are defined with a uniform distribution with a 5% variation around their mean. For this multi-parameter problem, sparse grids are used in order to reduce the number of samples to 871 allowing an acceptable computational time.

3. UQ on fan operating conditions

One-dimensional results on the operating conditions are first analyzed in Figure. 4 showing the iso-contours of the standard deviation from the 9 samples used in the SC method for each variable (volume flow rate and rotational speed), on the suction and pressure side of the blade. The two considered parameters are influencing different zones of the blade surface. For the volume flow rate, a large standard deviation is observed on the suction side of the airfoil, especially at the tip of the blade near the trailing-edge region, owing to large variations of the recirculation zone under the rotating ring, as it has been already highlighted in the URANS and SAS simulations on this fan (Moreau *et al.* 2012). A second zone of large standard deviation is also observed at the hub on the pressure side corresponding to the flow detachment at the blade leading edge created by the blade cusp. In case of rotational speed variations, the standard deviation of the pressure presents large amplitudes on a broader part of the blade, on both sides, around the leading edge up to mid-chord. The volume flow rate thus mainly influences the size of

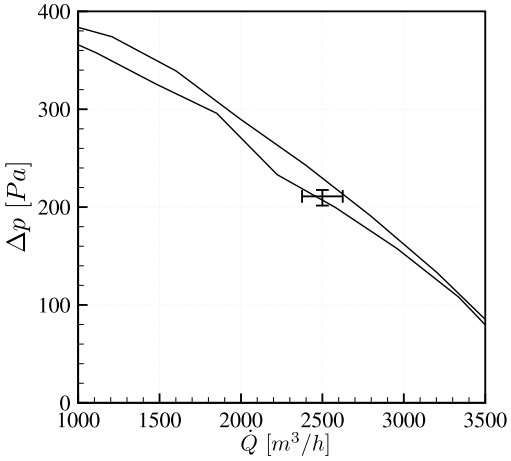

FIGURE 5. Fan performance.

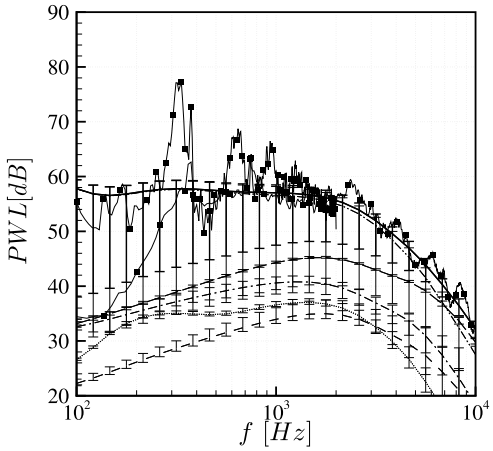

FIGURE 6. One-dimensional UQ on $\dot{Q}$. YR model, (solid bold) total sound, (dash) strip 1, (dash-dot) strip 2, (dot) strip 3, (long dash) strip 4, (dash-dot-dot) strip 5, (symbols) experiments.

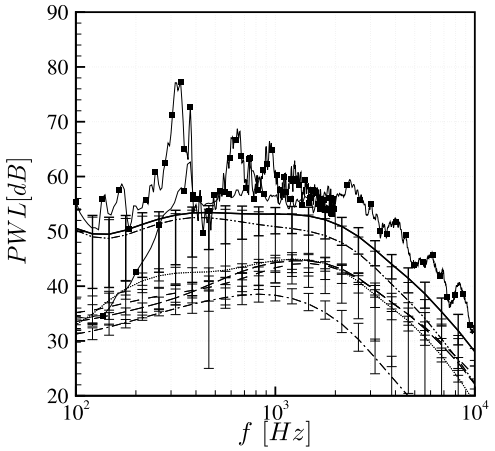

FIGURE 7. One-dimensional UQ on $\dot{Q}$. PL model, (solid bold) total sound, (dash) strip 1, (dash-dot) strip 2, (dot) strip 3, (long dash) strip 4, (dash-dot-dot) strip 5, (symbols) experiments.

the recirculation zones while the rotational speed modifies the complete blade pressure distribution.

A comparison of the fan overall performances with the error bar emphasizing the uncertainty interval in case of $\dot{Q}$ variations is presented in Figure. 5 for the pressure rise. Two experimental curves are provided as they represent the maximum experimental range of variations obtained on this fan between the many mock-ups and prototypes tested. It should be stressed that the error range on the volume flow rate was chosen to cover the experimental uncertainty, and the resulting uncertainty range on the pressure rise matches the experimental scattering well.

In Figures. 6 to 12, the spectra of the total simulated sound PoWer Level (PWL) for both YR and PL models are compared with two sets of experimental data, one

collected on an engine cooling module in a semi-anechoic chamber and one collected in a reverberant wind tunnel. Both models yield good agreement with the experimental broadband spectra stressing the significant contribution of this mechanism at design condition. The PL model presents a small under-prediction of about 3 dB over the whole frequency range, but a better overall shape especially at low frequencies compared to the reverberant wind tunnel data.

Figures. 6 and 7 provide the one-dimensional UQ results for a variation of $\dot{Q}$ for the YR and PL models respectively. The simulated PWL corresponding to the different strips discretizing the blade are shown together with their uncertainty bars. As shown in Moreau *et al.* (2012), the obtained sound spectra have shapes, amplitudes, and uncertainties similar to the trailing-edge wall-pressure spectra, indicating a direct propagation of the amplitudes and uncertainties through the noise propagation model. Larger uncertainties are obtained in the hub and tip regions as observed previously. The largest uncertainty bars at low frequencies in the tip region correspond to the large standard deviations seen in Figure. 4 and are related to the local large-scale flow separation under the fan ring. In the PL model, some lack of convergence in the integration of Eq. (2.2) by a Monte Carlo method could also contribute. At the hub, the largest uncertainties could be traced to the small scale structures created by the blade cusp. The total sound radiated by the complete blade is mainly caused by the noise emitted by the tip strip 5 with almost similar mean amplitudes. At high frequencies, the strip 4 also contributes to the total sound spectrum for the YR model whereas almost all blade strips contribute to the PL model. Moreover, the uncertainty bars for the complete blade are reduced compared with those of the tip strip. The complete fan noise spectrum is thus dominated in amplitude by the tip region while the uncertainty bars are related to uncertainties observed along the complete blade span. A proper control of the flow along the complete blade span is then necessary to reduced the uncertainties on the radiated sound. Finally, the PL model seems to yield lower overall uncertainty than the YR model. Figures. 8 and 9 show the corresponding one-dimensional UQ results for a variation of Ω for both YR and PL models. The same mean total spectrum dominated by the tip strip is obtained. The uncertainties (less than 1 dB) are, however, much smaller than for a variation of flow rate. Therefore, the process dispersion on the rotational speed does not trigger significant uncertainties on the fan trailing-edge noise.

Figures. 10 and 11 show the corresponding two-dimensional UQ results for variations of both $\dot{Q}$ and Ω for the YR and PL models respectively. A similar mean total spectrum dominated by the tip strip is again obtained. The uncertainty bars for both models now lie in between both one-dimensional UQ results on each separate performance parameter, yielding 2 to 6 dB for the YR model and 3 to 4 dB. The PL model therefore gives smaller uncertainties than the YR model, more uniformly spread over the whole frequency range.

4. UQ on post-processing and noise propagation methods

As discussed in Section. 2, a second source of uncertainty comes from all the parameters that are introduced in the data processing from the RANS data extraction to the noise prediction as described in Figure. 1. The determinitic RANS computation at nominal conditions is taken as a reference flow field, and only the YR model with the 9 stochastic parameters described in Section. 2.3 is considered here. As a full tensor grid with 9 CC

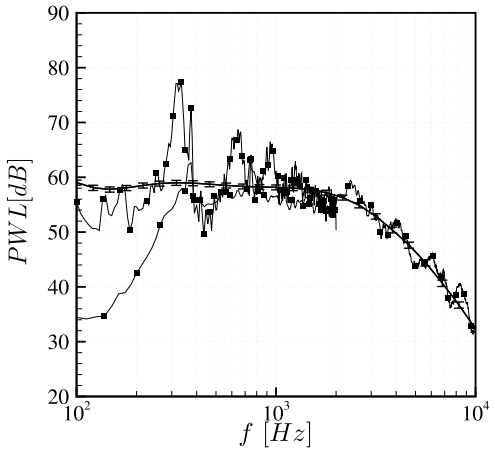

FIGURE 8. One-dimensional UQ on Ω. YR model, (solid) total sound, (symbols) experiments.

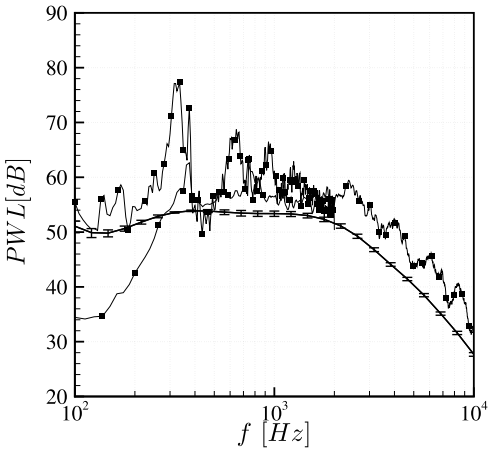

FIGURE 9. One-dimensional UQ on Ω. PL model, (solid) total sound, (symbols) experiments.

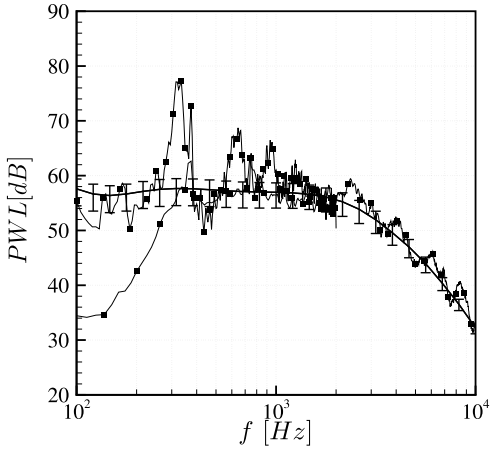

FIGURE 10. Two-dimensional UQ. YR model, (solid) total sound, (symbols) experiments.

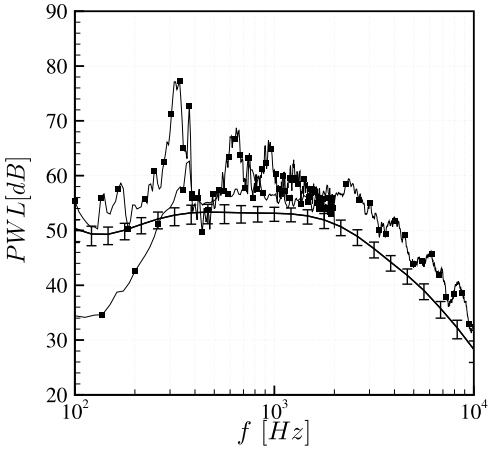

FIGURE 11. Two-dimensional UQ. PL model, (solid) total sound, (symbols) experiments.

points for each parameter would yield an unrealistic number of simulations, a sparse grid is used instead.

The final multi-parameter UQ result is shown in Figure. 12. Small constant uncertainties (a 5% variation around their mean) on the combined 9 parameters yield small sound uncertainty. Similar uncertainties, within 1 dB, were also obtained with a one-dimensional UQ on the separate parameters. Therefore, provided the model coefficients are known with some certainty, the predicted noise post-processing introduces little uncertainty

5. Conclusions

An uncertainty quantification has been achieved for the first time on the self-noise prediction of a low-subsonic axial fan, for which detailed experimental aerodynamic and

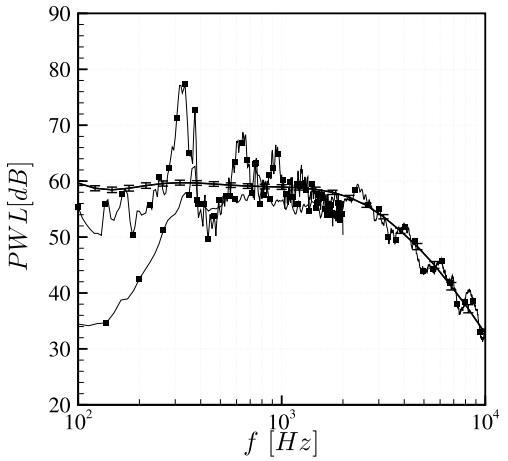

FIGURE 12. Multi-parameter UQ on YR model.

acoustic data as well as many steady and unsteady simulations exist. Both experimental and numerical data show some significant variations even at the design conditions. To account for the actual experimental and process scattering, realistic 5% and 4% errors about the mean are introduced on the volume flow-rate and the rotational speed respectively, and a maximum set of 9 steady RANS simulations of the fan mounted on a typical industrial test plenum has been simulated for each parameter, yielding a 81 full tensor-grid, to quantify the uncertainties on the resulting flow field using the SC method.

Extractions from this set of RANS simulations help to determine the uncertainty interval on global performances, boundary-layer profiles, wall-pressure distribution, and far-field noise spectra. The uncertainty bars obtained on the overall pressure rise match the experimental scattering quite well. By looking at the flow topology and particularly at the wall-pressure field, the variations are mainly located in the tip region along the last extraction line under the fan rotating ring. This also corresponds to the discrepancies seen between the recent RANS, URANS and SAS (scaled-adaptative-simulation) results. The uncertainty bars on the wall-pressure distribution and boundary-layer profiles show two different behaviors. On the one hand, close to hub and tip, large error bars are caused by the local flow separations. On the other hand, the other three sections bear similarities with the previous results on the CD airfoil from which this blade is constructed: flow attached over most of the blade chord with a growing boundary-layer caused by the adverse pressure gradient, except close to the leading-edge where the laminar flow separation introduces the largest uncertainties. Two models (PL and YR) are then used to reconstruct the trailing-edge wall-pressure spectra based on the RANS estimations of the turbulence. The latter are then the main inputs for the trailing-edge noise models based on Amiet's theory. The noise spectra obtained with both PL and YR models agree very well with two sets of experimental data on this fan, stressing the importance of this noise mechanism. The shapes, amplitudes, and uncertainties are similar to the trailing-edge spectra, showing a direct propagation of the amplitudes and uncertainties through the noise propagation model. The final noise spectra of the complete fan are dominated in amplitude by the tip region whereas the uncertainty bars are related to uncertainties observed along the complete blade span. A proper control of the flow along the complete blade span is then necessary to reduce the uncertainties on the radiated sound. The un-

certainties introduced by the variations on volume flow rate are much larger that those given by the rotational speed, and the combined effect of both fan parameters yields a 2-6 dB uncertainty on the far-field noise, with larger variations obtained with the YR model. Finally the effect of the various parameters involved in the fan noise prediction from RANS simulations has been achieved for the YR model at nominal operating conditions: provided a reasonable knowledge of their values (5% variation about the mean), the trailing-edge noise prediction is hardly affected (less than 1 dB).

Acknowledgments

The authors would like to thank the RQCHP consortium for providing HPC resources. The participation of the first author to the Summer Program is partially supported by the FP7-ECOQUEST project (Grant Agreement no 233541).

REFERENCES

Casalino, D., Moreau, S. & Roger, M. 2010 One, no one and one hundred thousand methods for low-speed fan noise prediction. *Int. J. Aeroacoustics* **3** (3), 307–327.

Christophe, J., Moreau, S., Hamman, C. W., Witteveen, J. A. S. & Iaccarino, G. 2010 Uncertainty quantification for the trailing-edge noise of a controlled-diffusion airfoil. In *Proceedings of the Summer Program 2010*. Centre for Turbulence Research, Stanford Univ./NASA Ames.

Christophe, J., Sanjosé, M. & Moreau, S. 2012 Uncertainty quantification of a low-speed axial fan self-noise. In *Proceedings ISROMAC Conference 2012*.

Glegg, S., Morin, B., Atassi, O. & Reba, R. 2010 Using reynolds-averaged navier-stokes calculations to predict trailing edge noise. *AIAA J.* **48** (7), 1290–1301.

Lighthill, M. J. 1952 On sound generated aerodynamically. i. general theory. *Proc. R. Soc. L. Series A* **211** (1102), 564–587.

Moreau, S. 2009 Airfoil noise : Experimental database and hybrid approaches. In *Aerodynamic Noise from Wall-Bounded Flows*. von Karman Institute for Fluid Dynamics Lecture Series.

Moreau, S. & Roger, M. 2007 Competing broadband noise mechanisms in low-speed axial fans. *AIAA J.* **45** (1), 48–57.

Moreau, S., Sanjosé, M., Magne, S. & Henner, M. 2012 Aerocoustic predictions of a low-subsonic axial fan. In *Proceedings ISROMAC Conference 2012*.

Panton, R. L. & Linebarger, J. H. 1974 Wall pressure spectra calculations for equilibrium boundary layers. *J. Fluid Mech.* **65** (02), 261–287.

Remmler, S., Christophe, J., Anthoine, J. & Moreau, S. 2010 Computation of wall-pressure spectra from steady flow data for noise prediction. *AIAA J.* **48** (9), 1997–2007.

Roger, M. & Moreau, S. 2005 Back-scattering correction and further extensions of amiet's trailing-edge noise model. part 1: Theory. *J. Sound and Vib.* **286**, 477–506.

Rozenberg, Y., Moreau, S., Henner, M. & Morris, S. C. 2010 Fan trailing-edge noise prediction using rans simulations. In *16th AIAA/CEAS Aeroacoustics Conference*. AIAA-2010-3720.

Schlinker, R. H. & Amiet, R. K. 1981 Helicopter rotor trailing edge noise. NASA CR 3470.